Acta Cryst. (1999). A**55**, 840–854

X-ray diffraction in perfect $t \times l$ crystals. Rocking curves

Gunnar Thorkildsen* and Helge B. Larsen

Department of Mathematics and Natural Science, Stavanger College, Ullandhaug, 4091 Stavanger, Norway.
E-mail: gunnar.thorkildsen@tn.his.no

(*Received 11 January 1999; accepted 18 February 1999*)

Abstract

A general formalism, based on the Takagi–Taupin equations, for calculating rocking curves in perfect $t \times l$ crystals is presented. It includes nonsymmetrical scattering, refraction, and ordinary and anomalous absorption. t and l may be varied independently. In the limit of a semi-infinite crystal, the standard results from the fundamental theory are retrieved. For crystal dimensions less than the extinction length, the theory converges to the kinematical limit. Simulations for germanium and silicon show significant influence of crystal finiteness. When dynamical effects are prominent, the curves exhibit various degrees of asymmetry and the full width at half-maximum is generally larger than the corresponding Darwin width. This is attributed to combined Laue and Bragg contributions which are shifted with respect to each other owing to refraction.

1. Introduction

Calculation of rocking curves for perfect crystals is commonly based on the fundamental theory of dynamical scattering (Darwin, 1914; Ewald, 1916*a*,*b*, 1917; Prins, 1930; von Laue, 1931; Ewald, 1937) with an incoming plane wave impinging a *semi-infinite* crystal plate (Zachariasen, 1945; von Laue, 1960; James, 1962; Batterman & Cole, 1964; Kato, 1974; Pinsker, 1978; Authier, 1996). In a series of papers (Thorkildsen & Larsen, 1998*a*,*b*,*c*, 1999; Larsen & Thorkildsen, 1998), we have discussed primary extinction and absorption in *finite* perfect crystals. In the following, we extend our treatment to include rocking curves as well. To our knowledge, the only rigorous attempt to calculate dynamical rocking curves in finite crystals is due to Olekhnovich & Olekhnovich. They performed calculations for symmetrical scattering in perfect crystals with square and cylindrical cross sections (Olekhnovich & Olekhnovich, 1978, 1980). The results were however only obtained for a limited range of the scattering angle and over a small angular interval. Zachariasen (1967) and Becker & Coppens (1974), in their works on extinction, developed a formalism also suitable for calculation of rocking curves for perfect convex crystals within the framework of the kinematical theory.

In the present work, we consider rocking curves for crystals with a rectangular $t \times l$ cross section. t and l may be varied independently. The treatment includes ordinary and anomalous absorption. Allowance for nonsymmetrical scattering geometry† is also made (Wilkins, 1978, 1981).

The basis of our calculations is the Takagi–Taupin equations (Takagi, 1962, 1969; Taupin, 1964), which are solved using the method of Riemann (Sommerfeld, 1949) combined with the boundary-value Green-function technique. Our approach is inspired by the treatises of Uragami (1969, 1970, 1971) and Becker (Becker, 1977; Becker & Dunstetter, 1984).

2. Theory

The formalism used in this work is the same as the one presented in the papers by Thorkildsen & Larsen (1998*b*), hereafter called TL-A, Thorkildsen & Larsen (1998*c*), TL-B, and Thorkildsen & Larsen (1999), TL-C. Definitions of variables and parameters are summarized in Appendix *A*.

The Takagi–Taupin equations for a perfect crystal are written in the representation [TL-A(6), (7)]

$$\partial \tilde{D}_o / \partial s_o = i\kappa_{oh}\, \tilde{D}_h \tag{1}$$

$$\partial \tilde{D}_h / \partial s_h = i\kappa_{ho}\, \tilde{D}_o. \tag{2}$$

By application of the Riemann–Green technique, the amplitude of the diffracted beam at a point P within the crystal is expressed by the integral equation [TL-A(12)]

$$D_{\mathbf{k}_h}(P) = \frac{i\kappa_{ho} D_o^{(e)}}{\sin 2\theta_{oh}} \int_{S(P)} \mathbf{s}_o \cdot \mathrm{d}\mathbf{S}\, G_h(u_0|\Delta_o, \Delta_h) \times \exp(2\pi i \alpha_h \Delta_h) \exp[-\pi i K \chi_o(\Delta_o + \Delta_h)]. \tag{3}$$

$i\kappa_{ho} G_h(u_0|\Delta_o, \Delta_h)$ is the boundary-value Green function, the solution of the equations for the diffracted field subject to the boundary condition $\tilde{D}_o^{(b)}(S) = \delta[s_h - s_h(S)]$. The Green function represents the propagation of the field incorporating all scattering–rescattering events along the possible optical routes

† In the present work, we do not consider the case of specularly reflected waves (Afanasev & Melkonyan, 1983; Alexandrov *et al.*, 1984; Holý, 1996), thus the angle of the incident wave to the surface is always much larger than the critical angle for total external reflection.

© 1999 International Union of Crystallography
Printed in Great Britain – all rights reserved

connecting the source point S and the point P. $u_0 = \kappa_{oh}\kappa_{ho}$ is the coupling parameter. It is in general a complex quantity owing to anomalous-scattering processes. The surface integral in equation (3) covers the part of the entrance surface where a source point can give rise to a displacement field at P. Δ_o and Δ_h are difference coordinates between the two points along $\mathbf{s}_o$ and $\mathbf{s}_h$. The excitation error, α_h, is associated with the deviation from the Bragg condition, $\Delta\theta_{oh}$, by equation (39). The real and imaginary components of the mean electric susceptibility, χ_o, are explicitly taken into account by introducing the phase factor, Q_h, and the factor A_h, related to ordinary absorption:

$$Q_h(\Delta_o, \Delta_h) = \exp(-2\pi i K \sin 2\theta_{oh} \Delta\theta_{oh} \Delta_h) \times \exp[\pi i K |\Re\chi_o|(\Delta_o + \Delta_h)] \quad (4)$$

$$A_h(\Delta_o, \Delta_h) = \exp[-\pi K |\Im\chi_o|(\Delta_o + \Delta_h)]. \quad (5)$$

The *intensity* at an exit point M is then written:

$$I_h(M, \Delta\theta_{oh}) = |D_{\mathbf{k}_h}(M)|^2 = I_o^{(e)} |\kappa_{ho}|^2 (1/\sin^2 2\theta_{oh}) \left| \int_{S(M)} \mathbf{s}_o \cdot \mathrm{d}\mathbf{S} \times G_h(u_0|\Delta_o, \Delta_h) Q_h(\Delta_o, \Delta_h) A_h(\Delta_o, \Delta_h) \right|^2 \quad (6)$$

and the *power*:

$$P_h(\Delta\theta_{oh}) = \int_M \mathbf{s}_h \cdot \mathrm{d}\mathbf{M} |D_{\mathbf{k}_h}(M)|^2 = I_o^{(e)} |\kappa_{ho}|^2 (1/\sin^2 2\theta_{oh}) \int_M \mathbf{s}_h \cdot \mathrm{d}\mathbf{M} \left| \int_{S(M)} \mathbf{s}_o \cdot \mathrm{d}\mathbf{S} \times G_h(u_0|\Delta_o, \Delta_h) Q_h(\Delta_o, \Delta_h) A_h(\Delta_o, \Delta_h) \right|^2. \quad (7)$$

$\mathrm{d}\mathbf{S} = \hat{\mathbf{s}}\,\mathrm{d}S$ and $\mathrm{d}\mathbf{M} = \hat{\mathbf{m}}\,\mathrm{d}M$ are oriented area elements of the entrance and exit surfaces. The unit normal vectors, $\hat{\mathbf{s}}$ and $\hat{\mathbf{m}}$, point into and out of the surfaces, respectively. For a semi-infinite rectangular crystal, *cf.* §2.2, the intensity is assumed not to vary across the area of the exit surface, $\mathcal{A}$, which is monitored. The associated power becomes†

$$P_h(\Delta\theta_{oh}) = \mathcal{A} \times (\mathbf{s}_h \cdot \hat{\mathbf{m}}) I_h(\Delta\theta_{oh}). \quad (8)$$

The variation of P_h with $\Delta\theta_{oh}$ is known as the rocking curve.

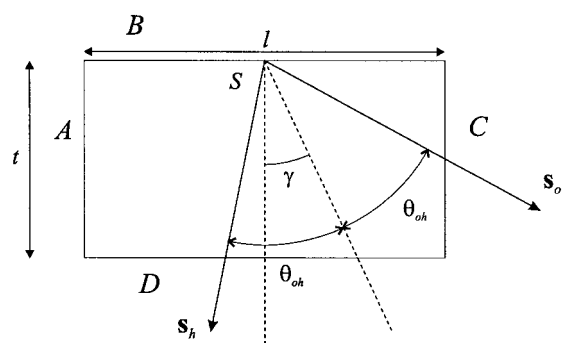

Fig. 1. Crystal dimensions, surface labels and scattering geometry.

2.1. *Finite crystals*

Fig. 1 gives geometrical definitions for the finite crystals in question. $S \in (A, B)$ and $M \in (A, D)$. Fig. 2 shows an example of the geometrical region structure associated with a source point, S, on the A and B entrance surfaces, respectively. These regions give the domains of applicability for the members of the Bragg and Laue families of Green functions, *cf.* TL-B, Section 2.4.2, TL-C, Section 2.3 and Saka *et al.* (1972*a*,*b*, 1973). At a given point on the exit surface, we add the amplitudes of the diffracted field originating from different source points. Depending on the position of the source, these contributions may belong to different regions, m, and are thus assigned to different Green functions. The associated integration structure, crucially dependent on the parameter ζ, has been properly dealt with in TL-B, Section 2.5 and TL-C, Section 2.4. It must be emphasized that, in the calculation of integrated power, the scattering contributions $i - j$ can be treated independently. In the present context, however, the amplitudes associated with $A - j$ and $B - j$ scattering, $j \in (A, D)$, must be summed prior to the integration over the exit surfaces. This causes a slight change in the integration set-up from that previously presented, *cf.* Thorkildsen & Larsen (1998*d*). It is convenient to use dimensionless coordinates (x, y) and dimensionless parameters‡ (u, ζ, ξ_0, μ_0) to simplify the integrand and the integration limits. The details concerning definitions of coordinates are given in Appendices *A* of TL-B and TL-C.

We write:

$$P_h(\Delta\theta_{oh}) = I_o^{(e)} |\kappa_{ho}|^2 v(l/2 \sin\theta_{oh}) P_h^{(0)}(\Delta\theta_{oh}), \quad (9)$$

where we have introduced a dimensionless quantity, the so-called *intrinsic power*:

$$P_h^{(0)}(\Delta\theta_{oh}) \stackrel{\text{def}}{=} (1/2\zeta) \sum_{j=A,D} \int_{M_j(\zeta)} \mathrm{d}y \times \left| \sum_{i=A,B} \sum_{m=m'_{i-j}(y)} \int_{S_{i-j}(y,m)} \mathrm{d}x\, G_h^{i-j}(u|x, y|m) \times Q_h^{i-j}(x, y) A_h^{i-j}(x, y) \right|^2. \quad (10)$$

The rocking curves for finite crystals are calculated from this equation. The important feature is the phase factors associated with each scattering process $i - j$. They are labelled according to the location of the source and exit

† In this case, we omit M in the expression for the intensity.
‡ *Cf.* equations (28), (32), (38) and (48).

point. These factors incorporate effects owing to refraction and the deviation from the Bragg condition.

$$Q_h^{A-A}(x, y) \rightarrow Q_h^{A-A}(x) = \exp\{-\pi i \xi_0 [\Delta\theta_{oh} x - (\Delta\theta_{oh}^0/2) \times (1 + \beta_+/\beta_-)x]\} \quad (11)$$

$$Q_h^{B-A}(x, y) = \exp\big(-\pi i \xi_0 \{\Delta\theta_{oh} x - (\Delta\theta_{oh}^0/2) \times [(1 - \delta_+/\delta_-)x + 2\beta_-\delta_+ y]\}\big) \quad (12)$$

$$Q_h^{A-D}(x, y) = \exp\big(-\pi i \xi_0 \{\Delta\theta_{oh} x - (\Delta\theta_{oh}^0/2) \times [(1 + \beta_+/\beta_-)x + 2\beta_+\delta_- y]\}\big) \quad (13)$$

$$Q_h^{B-D}(x, y) \rightarrow Q_h^{B-D}(x) = \exp\big(-\pi i \xi_0 \{\Delta\theta_{oh} x - (\Delta\theta_{oh}^0/2) \times [(1 - \delta_+/\delta_-)x + 2\delta_+\zeta]\}\big). \quad (14)$$

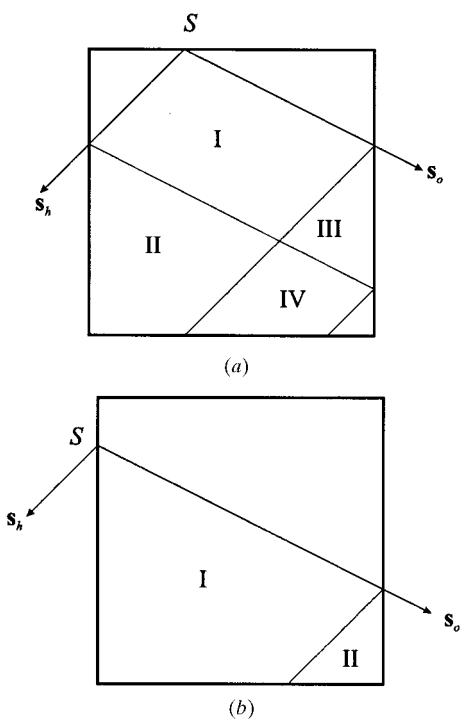

Fig. 2. (*a*) Laue and (*b*) Bragg families of regions.

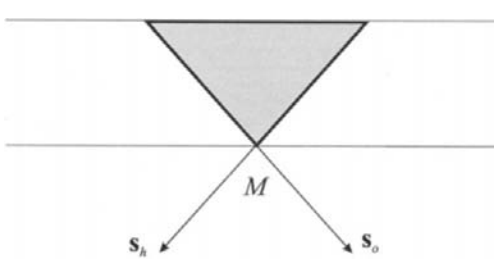

Fig. 3. Basic volume for Laue scattering.

When using equations (12)–(14) in equation (10), the absolute value of the factors $\exp(\pi i \Delta\theta_{oh}^0 \xi_0 \beta_- \delta_+ y)$, $\exp(\pi i \Delta\theta_{oh}^0 \xi_0 \beta_+ \delta_- y)$ and $\exp(\pi i \Delta\theta_{oh}^0 \xi_0 \delta_+ \zeta)$ is reduced to 1.

2.2. *Semi-infinite crystals*

In this section, we will use the formalism outlined for a finite perfect crystal to derive the basic expressions for the diffracted intensity from a semi-infinite specimen. The equivalence between the results obtained from the Takagi–Taupin equations and those from the fundamental theory (Pinsker, 1978; Authier, 1996) is shown in the limit of zero absorption in Appendix *B*. The formulas given represent nonsymmetrical scattering. The final expressions used for numerical calculations of reference curves are equations (16), (18) and (20) below. They may be used as alternatives to well established expressions based on the fundamental theory, *cf.* Kato (1992). The formulas are functions of the dimensionless variables η_L (Laue case) and η_B (Bragg case), *cf.* equations (42) and (43). Conversion to the $\Delta\theta_{oh}$ scale is obtained by

$$\Delta\theta_{oh} = -\frac{\lambda}{\pi \Lambda_{oh} \sin 2\theta_{oh}} \times \begin{cases} (\delta_+/\delta_-)^{1/2} \eta_L \\ (\beta_+/\beta_-)^{1/2} \eta_B \end{cases}.$$

2.2.1. *Laue case*. Fig. 3 shows the basic volume associated with Laue scattering. The actual Green function is

$$G_h^{B-D}(u|x|1) = J_0\big(2\{u[2\delta_+\zeta - (\delta_+/\delta_-)x]x\}^{1/2}\big).$$

Since no lateral boundaries limit the wave propagation, the expressions for the diffracted field amplitude and the intensity do not depend upon the position y of the exit point M. The amplitude of the displacement field is expressed by

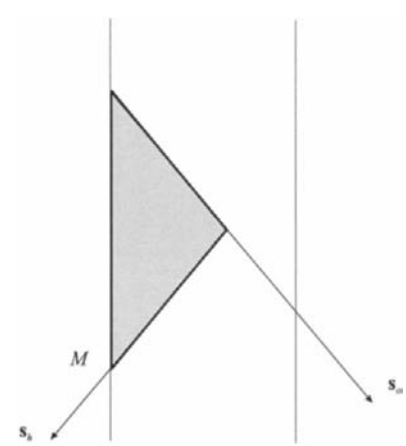

Fig. 4. Basic volume for Bragg scattering – Darwin limit.

$$D_{\mathbf{k}_h} = i\kappa_{ho}\ell D_o^{(e)} \int_0^{2\delta_-\zeta} \mathrm{d}x\, G_h^{B-D}(u|x|1) \times \exp(2\pi i\alpha_h \ell x) \exp\{-\pi i K \chi_o \times [(1-\delta_+/\delta_-)x + 2\delta_+\zeta]\ell\}. \quad (15)$$

Introducing η_L, the parameters ξ_L, $\Delta\eta_L$, μ_L, $\Delta\mu_L$ according to equations (36), (45), (50), (51) and changing integration variable

$$z = x/2\zeta\delta_-,$$

we obtain the following expression for the intensity (*cf.* Authier & Simon, 1968):

$$I_h(\eta_L) = I_o^{(e)}(|\kappa_{ho}|/|\kappa_{oh}|)(\delta_-/\delta_+)\exp(-\mu_L\xi_L) \times \left|\xi_L \int_0^1 \mathrm{d}z\, J_0\{2\xi_L[(1-z)z]^{1/2}\exp(i\Phi_0)\} \times \exp[2i\xi_L(\eta_L - \Delta\eta_L)z]\exp(-\Delta\mu_L\xi_L z)\right|^2. \quad (16)$$

2.2.2. *Bragg case – Darwin solution*. Fig. 4 gives the volume for Bragg scattering in the Darwin limit. It is essential that the scattering volume does not encounter the 'back' surface of the crystal.† In addition, the coordinate of the exit point M should extend to infinity if the standard top-hat shape (Darwin, 1914) for the diffracted intensity function is to be obtained. The entire scattering volume belongs to the region $m = 1$ associated with A–A scattering. The actual Green function thus becomes:

$$G_h^{A-A}(u|x|1) = J_0\left[2\left(u\frac{\beta_+}{\beta_-}\right)^{1/2}x\right] + J_2\left[2\left(u\frac{\beta_+}{\beta_-}\right)^{1/2}x\right]$$

and the field amplitude is:

$$D_{\mathbf{k}_h} = \lim_{y\to\infty} i\kappa_{ho}\ell D_o^{(e)} \int_0^{(\beta_-/\beta_+)y} \mathrm{d}x\, G_h^{A-A}(u|x|1) \times \exp(2\pi i\alpha_h\ell x)\exp\left[-\pi i K\chi_o\left(1+\beta_+/\beta_-\right)\ell x\right]. \quad (17)$$

Introducing η_B, the parameters $\Delta\eta_B$, μ_B according to equations (46), (52) and changing integration variable,

$$z = (2\ell/\Lambda_{oh})(\beta_+/\beta_-)^{1/2}x,$$

we obtain the intensity of the diffracted wave as

$$I_h(\eta_B) = I_o^{(e)}(|\kappa_{ho}|/|\kappa_{oh}|)(\beta_-/\beta_+) \times \left|\tfrac{1}{2}\int_0^\infty \mathrm{d}z\, \{J_0[z\exp(i\Phi_0)] + J_2[z\exp(i\Phi_0)]\} \times \exp[i(\eta_B - \Delta\eta_B)z]\exp(-\mu_B z)\right|^2. \quad (18)$$

† This is in popular terms the definition of a 'thick' crystal.

2.2.3. *Bragg case – Ewald solution*. The basic regions giving the Ewald solution for Bragg scattering (Zachariasen, 1945) are shown in Fig. 5. Now the field propagation experiences the effects of the 'back' surface creating an in principle infinite region structure. In the limit when M approaches infinity, we can express the field amplitude by

$$D_{\mathbf{k}_h} = \lim_{p_{\max}\to\infty} i\kappa_{ho}\ell D_o^{(e)} \times \sum_{p=0}^{p_{\max}} \int_{2p\beta_-}^{(2p+2)\beta_-} \mathrm{d}x\, G_h^{A-A}(u|x|2p+1)\exp(2\pi i\alpha_h\ell x) \times \exp[-\pi i K\chi_o(1+\beta_+/\beta_-)\ell x], \quad (19)$$

i.e. we sum the contributions from each region. Introducing the parameter ξ_B and changing variable,

$$z = x/\beta_-,$$

we find:

$$I_h(\eta_B) = I_o^{(e)}(|\kappa_{ho}|/|\kappa_{oh}|)(\beta_-/\beta_+) \times \left|(\xi_B/2)\sum_{p=0}^{\infty}\int_{2p}^{(2p+2)} \mathrm{d}z\, G_h^{A-A}(\xi_B|z|2p+1) \times \exp[i(\eta_B - \Delta\eta_B)\xi_B z]\exp(-\mu_B\xi_B z)\right|^2, \quad (20)$$

or with $\bar{z} = \xi_B z$, we have:

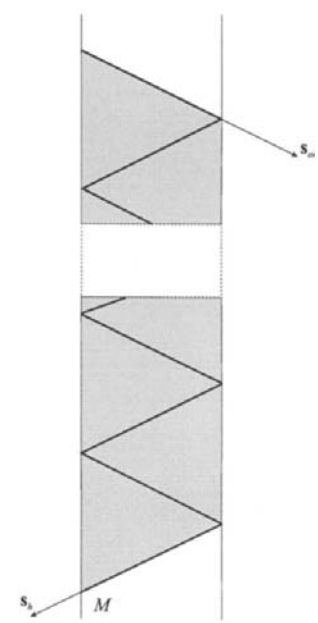

Fig. 5. Bragg scattering in the Ewald limit.

$$I_h(\eta_B) = I_o^{(e)}(|\kappa_{ho}|/|\kappa_{oh}|)(\beta_-/\beta_+) \times \left| \tfrac{1}{2}\int_0^\infty \mathrm{d}\bar{z}\,\{J_0[\bar{z}\exp(i\Phi_0)] + J_2[\bar{z}\exp(i\Phi_0)]\} \times \exp[i(\eta_B - \Delta\eta_B)\bar{z}]\exp(-\mu_B\bar{z}) + (\xi_B/2)\sum_{p=1}^{\infty}\int_{2p}^{\infty}\mathrm{d}z\, w_h^{A-A}(\xi_B|z|2p) \times \exp[i(\eta_B - \Delta\eta_B)\xi_B z]\exp(-\mu_B\xi_B z)\right|^2. \quad (21)$$

Equation (21) shows that the Ewald solution to the diffracted intensity is built from the Darwin solution, *cf.* equation (18), with addition of terms originating from the 'back' surface. To arrive at equation (21) from (20), we have used the following results for the Bragg family of Green functions, *cf.* Pinsker (1978, equation [11.76]):

$$G_h^{A-A}(\xi_B|z|2p+1) = G_h^{A-A}(\xi_B|z|2p-1) + w_h^{A-A}(\xi_B|z|2p)$$
$$G_h^{A-A}(\xi_B|z|1) = J_0[\xi_B z\exp(i\Phi_0)] + J_2[\xi_B z\exp(i\Phi_0)]$$

$$w_h^{A-A}(\xi_B|z|2p) = (-1)^p\left[\left(\frac{z-2p}{z+2p}\right)^{p-1} \times J_{2p-2}\{\xi_B[z^2-(2p)^2]^{1/2}\exp(i\Phi_0)\} + 2\left(\frac{z-2p}{z+2p}\right)^{p} J_{2p}\{\xi_B[z^2-(2p)^2]^{1/2} \times \exp(i\Phi_0)\} + \left(\frac{z-2p}{z+2p}\right)^{p+1} \times J_{2p+2}\{\xi_B[z^2-(2p)^2]^{1/2}\exp(i\Phi_0)\}\right].$$

2.3. *Kinematical limit*

The kinematical limit is obtained for $u \to 0$, *i.e.* the ratio of characteristic length, ℓ, to extinction length, Λ_{oh}, tends to zero. This ensures that the diffracted field is built from single scattering events only. The regions that contribute in this limit are $m = 1$ associated with Bragg scattering (source point on surface A) and $m = 1, 2$ associated with Laue scattering (source point on surface B). The relevant Green functions are all equal to unity. Furthermore, $\Re\chi_o$ and $\Im\chi_o$ are set to zero. $P_h^{(0)}(\Delta\theta_{oh})$ in

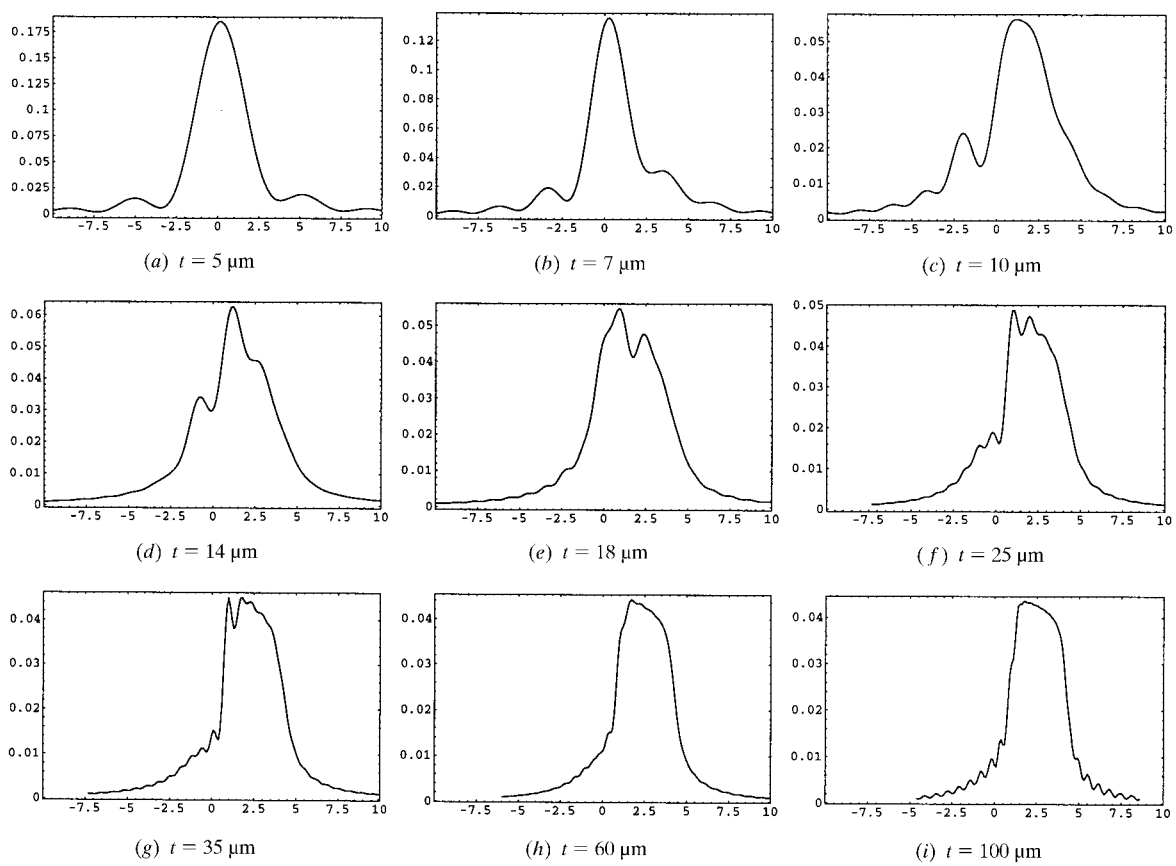

Fig. 6. Germanium (111), l = 5 μm, varying t.

the case of nonsymmetrical scattering is then given by equations (22) and (23) below:
For $0 \le \zeta < \beta_-/\delta_-$:

$$P_h^{(0)} = (1/2\zeta)\left[\int_0^{\zeta/\beta_-} \mathrm{d}y \left|\int_0^{2\beta_-\delta_- y} \mathrm{d}x \exp(-\pi i \xi_0 \Delta\theta_{oh} x)\right|^2 + \int_0^{1/\delta_- - \zeta/\beta_-} \mathrm{d}y \left|\int_0^{2\delta_-\zeta} \mathrm{d}x \exp(-\pi i \xi_0 \Delta\theta_{oh} x)\right|^2 + \int_{1/\delta_- - \zeta/\beta_-}^{1/\delta_-} \mathrm{d}y \left|\int_0^{2\beta_- - 2\beta_-\delta_- y} \mathrm{d}x \exp(-\pi i \xi_0 \Delta\theta_{oh} x)\right|^2\right]$$
$$= [2\pi\xi_0\delta_-\zeta\Delta\theta_{oh} + 2\pi\xi_0\Delta\theta_{oh}(\beta_- - \delta_-\zeta) \times \sin^2(\pi\xi_0\delta_-\zeta\Delta\theta_{oh}) - \sin(2\pi\xi_0\delta_-\zeta\Delta\theta_{oh})] \times [(\pi\xi_0\Delta\theta_{oh})^3\beta_-\delta_-\zeta]^{-1}. \quad (22)$$

For $\zeta \ge \beta_-/\delta_-$:

$$P_h^{(0)} = (1/2\zeta)\left[\int_0^{1/\delta_-} \mathrm{d}y \left|\int_0^{2\beta_-\delta_- y} \mathrm{d}x \exp(-\pi i \xi_0 \Delta\theta_{oh} x)\right|^2 + \int_{1/\delta_-}^{\zeta/\beta_-} \mathrm{d}y \left|\int_0^{2\beta_-} \mathrm{d}x \exp(-\pi i \xi_0 \Delta\theta_{oh} x)\right|^2 + \int_0^{1/\delta_-} \mathrm{d}y \left|\int_0^{2\beta_- - 2\beta_-\delta_- y} \mathrm{d}x \exp(-\pi i \xi_0 \Delta\theta_{oh} x)\right|^2\right]$$
$$= [2\pi\xi_0\beta_-\Delta\theta_{oh} - 2\pi\xi_0\Delta\theta_{oh}(\beta_- - \delta_-\zeta) \times \sin^2(\pi\xi_0\beta_-\Delta\theta_{oh}) - \sin(2\pi\xi_0\beta_-\Delta\theta_{oh})] \times [(\pi\xi_0\Delta\theta_{oh})^3\beta_-\delta_-\zeta]^{-1}. \quad (23)$$

Becker & Coppens (1974) extended the theory introduced by Zachariasen (1967) and gave a general formula for the diffracted power, P_k, for a convex perfect crystal in the kinematical limit. With their notation [equations (4), (*C*7)]:

$$P_k(\varepsilon_1) = I_o^{(e)} Q \int_v \mathrm{d}v\, \alpha \sin^2(\pi\varepsilon_1\alpha)/(\pi\varepsilon_1\alpha)^2, \quad (24)$$

where $\varepsilon_1 = \Delta\theta_{oh}$ and Q is the average scattering cross section per unit volume of the crystal. The parameter α is defined by $\alpha = l_h \sin 2\theta_{oh}/\lambda$ with l_h being the thickness of the crystal parallel to the diffracted beam. Applying this formalism to a rectangular crystal gives results identical to equations (22) and (23).

3. Results and discussion

The above presented theory was implemented in *Mathematica* version 3.0 (Wolfram, 1996).

As model systems for the simulations, we chose silicon and germanium. The structure factors were calculated at room temperature using atomic form factors from Waasmaier & Kirfel (1995) and anomalous-scattering corrections based on the program *FPRIME* (Cromer & Liberman, 1970; Cromer, 1995). All the calculations were performed at the wavelength $\lambda = 1.2$ Å, using $C = |\cos 2\theta_{oh}|$ for the polarization factor. Thus, only a single state of polarization is covered in this work. Table 1 summarizes some parameters for the reflections addressed. In the plots, Figs. 6–18, the abscissa, $\Delta\theta_{oh}$, is given in units of 10^{-3}°. The ordinate, $P_h^0(\Delta\theta_{oh})$ for finite

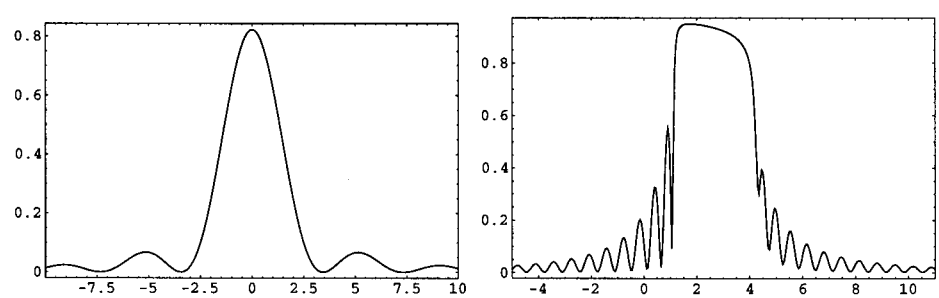

(*a*) Lauc (*b*) Bragg–Ewald

Fig. 7. Germanium (111), crystal thickness 5 μm.

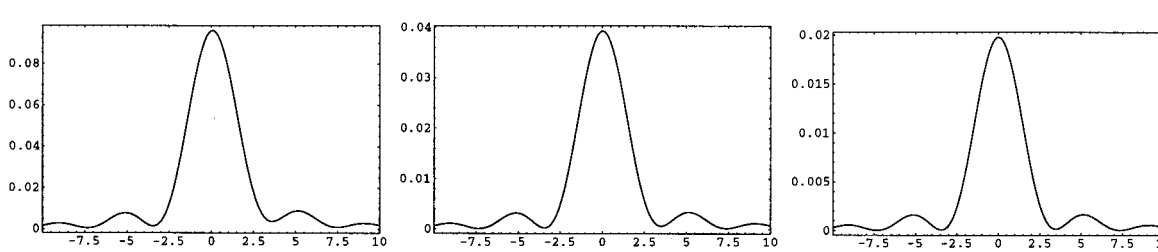

(*a*) $l = 10$ μm (*b*) $l = 25$ μm (*c*) $l = 50$ μm

Fig. 8. Germanium (111), $t = 5$ μm, varying l.

Table 1. *Some reflection parameters at* $\lambda = 1.2$ *Å*

θ_{oh}: Bragg angle. $\Delta\theta^0_{oh}$: shift in Bragg angle. Λ_{oh}: extinction length. $\delta_{\rm BE}$: Bragg–Ewald width.

Element	*hkl*	θ_{oh} (°)	$\Delta\theta^0_{oh}$ (10^{-3}°)	Λ_{oh} (μm)	$\delta_{\rm BE}$ (10^{-3}°)
Ge	111	10.584	2.69	4.10	3.22
Si	111	11.032	1.40	8.53	1.49
Si	333	33.034	0.558	41.1	0.123
Si	135	40.814	0.530	110	0.0209 ($\gamma > 0$) 0.0921 ($\gamma < 0$)

crystals, $I_h(\Delta\theta_{oh})/I_o^{(e)}$ for semi-infinite crystals, is in arbitrary units.

3.1. $t \times l$ *crystal cross section*

In order to exemplify and assess some features of dynamical rocking curves from perfect finite crystals, we present a set of simulations for different crystal geometries. Figs. 6(*a*)–(*i*) depict the rocking curves for a $t \times l$ cross section Ge crystal when l is kept constant equal to 5 μm and t is varied. The reflection studied was 111. With quite a large range of aspect ratios, we proceed from a Laue regime for low values of t/l (<2) *via* an 'intermediate' interval ($2 < t/l < 4$) to a Bragg dominated regime at large values of t/l (>4). In this context, we note the shift of the curves towards larger values of $\Delta\theta_{oh}$ as t/l increases. This is due to the refraction effect, a feature which for the symmetrical case is associated with Bragg scattering, *cf.* equations (11)–(14). The rocking curves should be compared with the Laue and Bragg–Ewald solution for a semi-infinite crystal plate given in Fig. 7. We notice that the rocking curves for small t/l values are broader than the Bragg–Ewald width, $\delta_{\rm BE} = (4 \times 6^{1/2}/9)\delta_D$. δ_D is the well known Darwin width, see for instance Coppens (1992). This however critically depends upon the value of t/l. As this ratio grows, the full width at half-maximum (FWHM) of the rocking curves gradually decreases towards the Bragg–Ewald width.

In Fig. 8, t is constant equal to 5 μm and l varies. The shape of the rocking curves is rather insensitive to this variation, since no new geometrical regions are created with increasing l. Thus, Laue scattering associated with region $m = 1$ dominates.

3.2. $t \times t$ *crystal cross section*

In Figs. 9 and 10, we have shown the results for the Ge and Si 111 reflection in a square cross section ($t \times t$) crystal. For germanium, the Laue and Bragg–Darwin solutions for a crystal plate of thickness 40 μm are shown in Fig. 11. Fig. 12 shows the Laue and Bragg–Ewald solutions for silicon for the same geometry. Overall features are well described with a Laue curve superimposed on a smooth Bragg–Darwin background. To address the effect of the mixed scattering terms ($A - D$ and $B - A$), we have in Fig. 13 plotted the difference between two calculated rocking curves with these terms respectively included or not included. It is seen that for a squaric crystal cross section and symmetrical diffraction the main contributions from

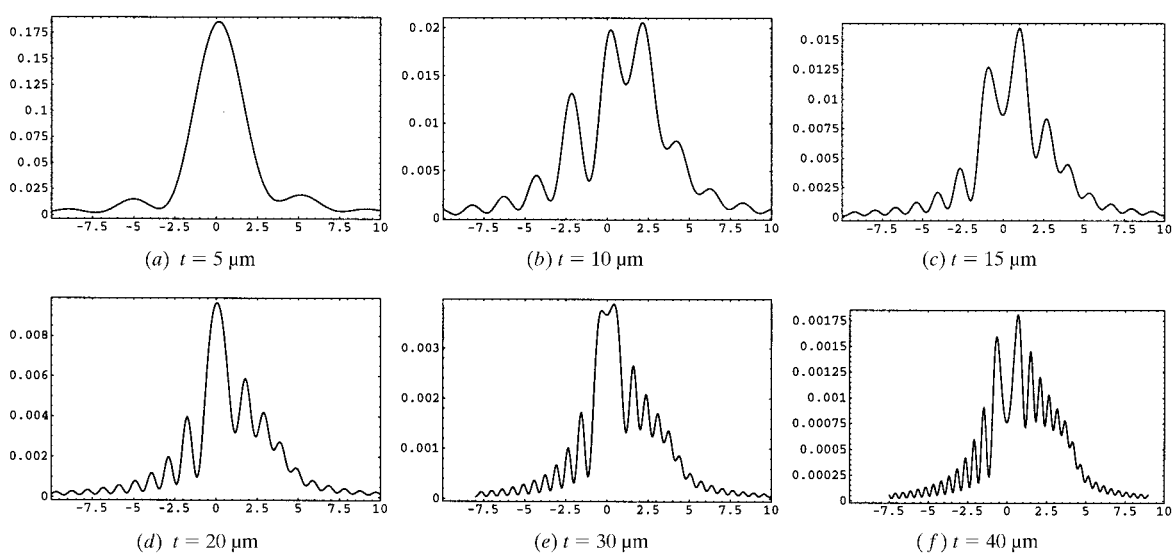

Fig. 9. Germanium (111), $t \times t$ crystal, varying t.

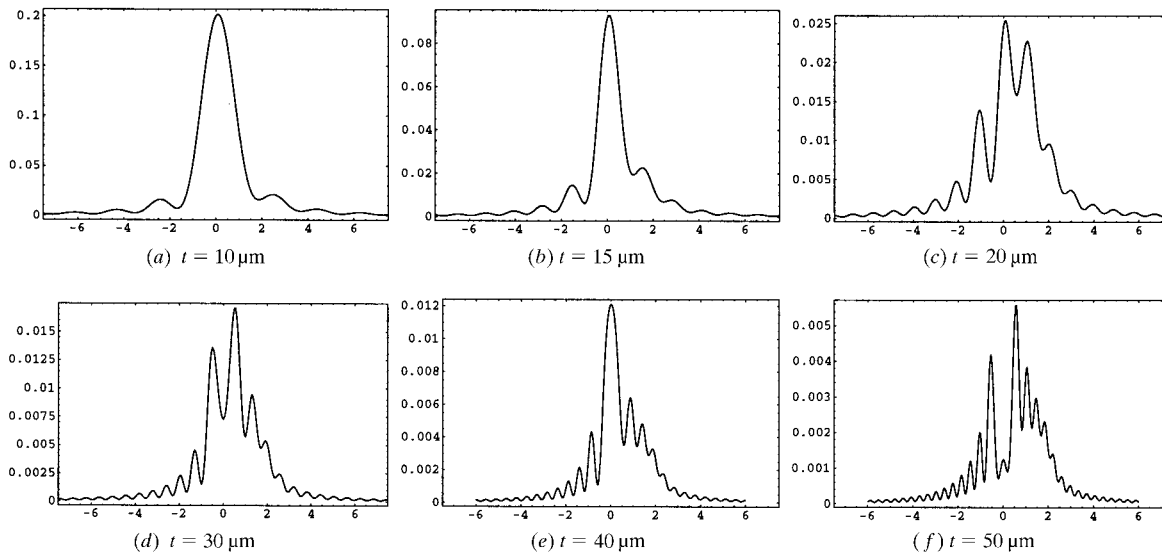

Fig. 10. Silicon (111), $t \times t$ crystal, varying t.

mixed terms occur in the central regions of the rocking curves.

For comparison with a real experiment, the intrinsic dynamical rocking curves should be convoluted with a smearing function representing the incoming beam divergence. Assuming synchrotron radiation from a bending magnet, we use a Gaussian with FWHM equal to $1.5 \times 10^{-3\circ}$. The results of this convolution are shown for germanium in Fig. 14. We observe that the rocking curves retain an asymmetrical shape owing to finite crystal dynamical effects – *i.e.* the joint Laue and Bragg scattering contributions separated due to refraction. A significant peak splitting owing to such effects is seen by studying the Si 333 reflection – *cf.* Fig. 15. Depending on the crystal size, the relative strength of the Laue and Bragg peaks is interchanged.

3.3. *Effect of reflection asymmetry*

So far we have only addressed cases involving symmetrical reflections. The algorithms for calculating the rocking curves are, however, general and include the possibility of having a nonsymmetrical reflection as well.† An example is shown for the Si 135 reflection ($t \times t$ crystal geometry) which has an asymmetry angle‡ $|\gamma| = 28.561^\circ$. As seen in Fig. 16, this creates asymmetric rocking curves with a (small) buildup of power on the low-angle side of the main peak. This buildup develops into an auxiliary peak for increasing crystal size. Correspondingly, simulations for the *negative* nonsymmetrical case of the Si 135 reflection show increased power on the high-angle side, *cf.* Fig. 17. There is also a small shift in the position of the main peaks in the two cases. Here the dominant contributions are due to $A - D$ scattering (γ positive) and $B - A$ scattering (γ negative). For this reflection, $\Delta\theta_{oh}^0 = 0.53 \times 10^{-3\circ}$. When γ is positive, $\delta_+/\delta_- = 2.77$ and $\beta_+/\beta_- = 0.227$. A negative γ gives the inverse values for these ratios. The main peak in Fig. 16(f) is found for $\Delta\theta_{oh} \approx 0.33 \times 10^{-3\circ}$, in accordance with the shift calculated from equation (13). Similarly, for the negative case, the main peak is located at $\Delta\theta_{oh} \approx 0.17 \times 10^{-3\circ}$ in accordance with equation (12). The FWHM of the main peaks in the two cases is approximately equal and, for $t = 150\,\mu m$, FWHM $\approx 0.05 \times 10^{-3\circ}$. For the setting with negative γ, the comparison with the Bragg–Ewald width loses significance since this limit refers to multiregion $A - A$ scattering.§ The position of auxiliary maxima are $\Delta\theta_{oh} \approx -0.47 \times 10^{-3\circ}$ for $\gamma = +28.561^\circ$, corresponding to $B - A$ and $B - D$ scattering, and $\Delta\theta_{oh} \approx +1.43 \times 10^{-3\circ}$ for $\gamma = -28.561^\circ$, corresponding to $A - A$ and $A - D$ contributions. For increasing crystal size, the auxiliary peaks will decrease ($\gamma > 0$) and increase ($\gamma < 0$) with respect to the main peaks since pure Bragg scattering ($A - A$) becomes more dominant.

3.4. *The kinematical limit*

With the crystal dimensions reduced to $1 \times 1\,\mu m$, the rocking curves for the 111 reflections of germanium and silicon almost coincide. Now the crystal dimension is much smaller than the actual extinction lengths and the calculation approaches the kinematical limit of single

† The following conditions must be fulfilled: $|\gamma| \leq \theta_{oh}, \theta_{oh} \leq \pi/4$. Thus there is always a Bragg scattering regime present.

‡ The entrance surface A is oriented parallel to (111).

§ In fact, the width of the auxiliary peak at $\Delta\theta_{oh} \approx +1.43 \times 10^{-3\circ}$ approaches the Bragg–Ewald width for a crystal size larger than 1 mm.

scattering. $P_h^{(0)}$ then becomes independent of the expansion parameter, u_0, which is associated with multiple-scattering events. Fig. 18 gives the results for silicon 111 for the crystal dimensions: (*a*) $t \times l = 0.2 \times 1.0$ μm and (*b*) $t \times l = 1.0 \times 0.2$ μm. These simulations are in accordance with calculations based on equation (*C*7) of Becker & Coppens (1974). The variation of FWHM for rocking curves calculated in the kinematical limit for a $t \times t$ crystal is shown in Fig. 19.

Although the kinematical limit is reproduced within the present formalism, we would like to draw attention to the following point: In the derivation of the Takagi–Taupin equations, the electric susceptibility is expanded in a Fourier series assuming an in principle unbounded crystal which causes the coupling parameter, κ_{pq}, to be independent of crystal shape. This should encourage a careful re-examination of the derivation of the Takagi–Taupin equations with focus on crystal finiteness.

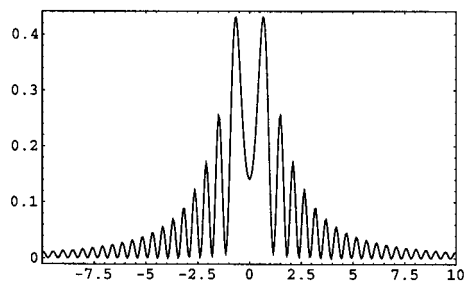

(*a*) Laue

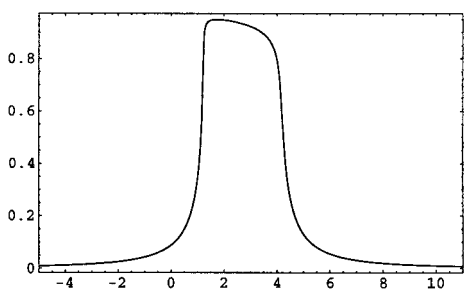

(*b*) Bragg–Darwin

Fig. 11. Germanium (111), crystal thickness 40 μm.

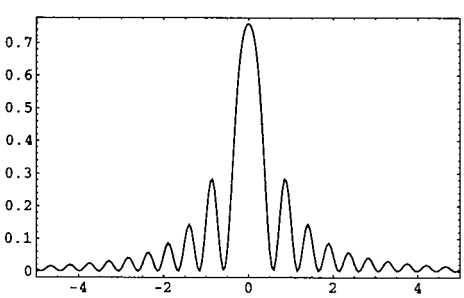

(*a*) Laue

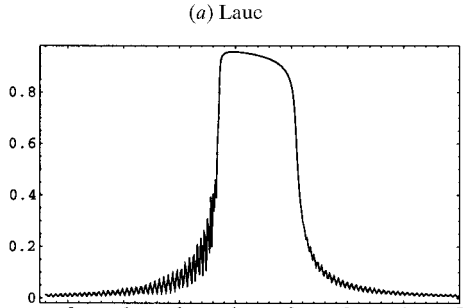

(*b*) Bragg–Ewald

Fig. 12. Silicon (111), crystal thickness 40 μm.

4. Conclusions

In this paper, we have successfully demonstrated how the Takagi–Taupin formalism can be used to calculate rocking curves from finite perfect crystals. It is verified that the traditional Laue and Bragg–Ewald/Bragg–Darwin solutions of the dynamical theory of X-ray scattering are obtained in the limit of a semi-infinite perfect-crystal plate. In addition, kinematical results in the limit of small crystal dimensions are retrieved. The results show significant profile asymmetries inherent in the dynamical contributions from finite crystals. The rocking curves often have a full width at half-maximum larger than the Bragg–Ewald width for corresponding semi-infinite samples. Different refraction effects and different relative contributions for Laue and Bragg scattering may lead to shifts in the peak positions.

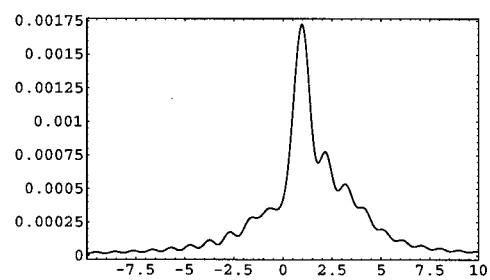

(*a*) Germanium

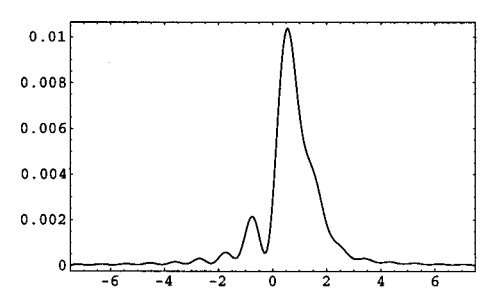

(*b*) Silicon

Fig. 13. Difference plots. Effects from mixed scattering terms. Reflection (111). Crystal dimensions: 20 × 20 μm.

Generally, the shape of the rocking curves deviates significantly from those predicted for semi-infinite crystals. Care must therefore be shown when analyzing experimental rocking curves from small perfect-crystal samples. For such cases, the Takagi–Taupin approach is more versatile because it explicitly embraces crystal finiteness.

The present implementation of the theory using *Mathematica* puts some practical limits on the cases that may be studied since the computing time increases very rapidly with increasing values of the parameters ζ, ξ_0 and u.

APPENDIX *A*
Definitions

*A*1. *General definitions*

The definitions of the parameters appearing in the paper are given in Table 2. Throughout this work, we have used 'crystallographic' notation, *i.e.* the mathematical representation of a plane wave is $\exp(-2\pi i\mathbf{K}\cdot\mathbf{r})$ with wavenumber $|\mathbf{K}| = K = 1/\lambda$.

*A*2. *Scattering parameters*

Fourier coefficient of the electric susceptibilty:

$$\chi_{p-q} = -(r_e\lambda^2/\pi V_c)F_{p-q}. \tag{25}$$

Coupling parameter:

$$\kappa_{pq} = -\pi KC\chi_{p-q} = (r_e\lambda C/V_c)F_{p-q} = |\kappa_{pq}|\exp(i\phi_{pq}). \tag{26}$$

Table 2. *Definitions of the parameters*

r_e	Classical electron radius
λ	Wavelength
V_c	Volume of unit cell
F_{p-q}	Structure factor for reflection $p-q$
C	Polarization factor $1 \vee \lvert\cos 2\theta_{oh}\rvert$
$\Re\chi_o$	Real part of average electric susceptibility
$\Im\chi_o$	Imaginary part of average electric susceptibility
v	Volume of crystal
θ_{oh}	Bragg angle
s_o	Coordinate along incident beam
s_h	Coordinate along diffracted beam
$D_o^{(e)}$	Amplitude of incoming plane wave
$I_o^{(e)}$	Intensity of incoming plane wave
$\tilde{D}_o$	Amplitude of transmitted wave
$\tilde{D}_h$	Amplitude of diffracted wave

Extinction length:

$$\Lambda_{oh} = 1/(|\kappa_{oh}||\kappa_{ho}|)^{1/2}. \tag{27}$$

Expansion parameter:

$$u = \kappa_{oh}\kappa_{ho}(l/2\sin\theta_{oh})^2. \tag{28}$$

Phase factor:

$$\Phi_0 = (\phi_{oh} + \phi_{ho})/2. \tag{29}$$

Darwin width:

$$\delta_D = \frac{2r_e\lambda^2 C|F_h|}{\pi V_c \sin 2\theta_{oh}}\left(\frac{\beta_+}{\beta_-}\right)^{1/2}. \tag{30}$$

Kinematical cross section per unit volume:

$$Q = |r_e F_h C/V_c|^2(\lambda^3/\sin 2\theta_{oh}). \tag{31}$$

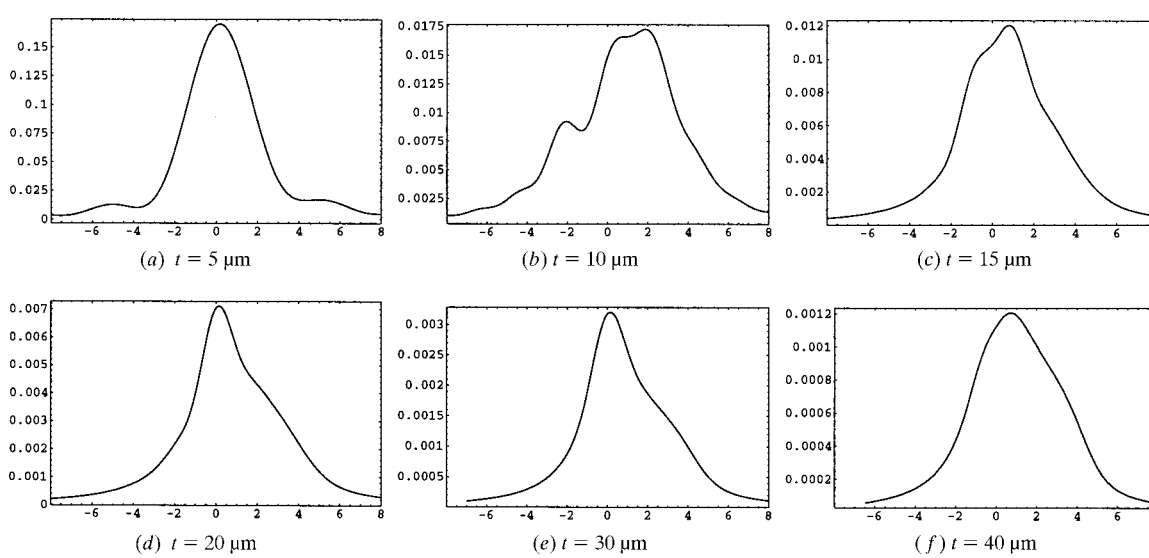

Fig. 14. Germanium (111), $t \times t$ crystal, convoluted rocking curves.

A3. Geometry related parameters

Basic parameters:

$$\zeta = (t/l)\tan\theta_{oh} \tag{32}$$

$$\ell = l/2\sin\theta_{oh} \tag{33}$$

$$\delta_{\pm} = \cos\theta_{oh}/\cos(\theta_{oh} \pm \gamma) \tag{34}$$

$$\beta_{\pm} = \sin\theta_{oh}/\sin(\theta_{oh} \pm \gamma). \tag{35}$$

Dimensionless length parameters:

$$\xi_L = (2\zeta\ell/\Lambda_{oh})(\delta_+\delta_-)^{1/2} \tag{36}$$

$$\xi_B = (2\ell/\Lambda_{oh})(\beta_+\beta_-)^{1/2} \tag{37}$$

$$\xi_0 = (2l/\lambda)\cos\theta_{oh}. \tag{38}$$

A4. Deviation parameters

Excitation error:

$$\alpha_h = -K\sin 2\theta_{oh}\Delta\theta_{oh}. \tag{39}$$

Shift in Bragg angle:

$$\Delta\theta^0_{oh} = |\Re\chi_o|/\sin 2\theta_{oh}. \tag{40}$$

Related parameters:

$$\eta_0 = \pi\alpha_h\Lambda_{oh} \tag{41}$$

$$\eta_L = \eta_0(\delta_-/\delta_+)^{1/2} \tag{42}$$

$$\eta_B = \eta_0(\beta_-/\beta_+)^{1/2} \tag{43}$$

$$\eta_\Lambda = -\pi K|\Re\chi_o|\Lambda_{oh} \tag{44}$$

$$\Delta\eta_L = \eta_\Lambda \tfrac{1}{2}[(\delta_-/\delta_+)^{1/2} - (\delta_+/\delta_-)^{1/2}] \tag{45}$$

$$\Delta\eta_B = \eta_\Lambda \tfrac{1}{2}[(\beta_+/\beta_-)^{1/2} + (\beta_-/\beta_+)^{1/2}]. \tag{46}$$

A5. Absorption parameters

Linear absorption coefficient:

$$\mu = 2\pi K|\Im\chi_o|. \tag{47}$$

Dimensionless absorption coefficients:

$$\mu_0 = \mu(l/2\sin\theta_{oh}) \tag{48}$$

$$\mu_\Lambda = \mu\Lambda_{oh}. \tag{49}$$

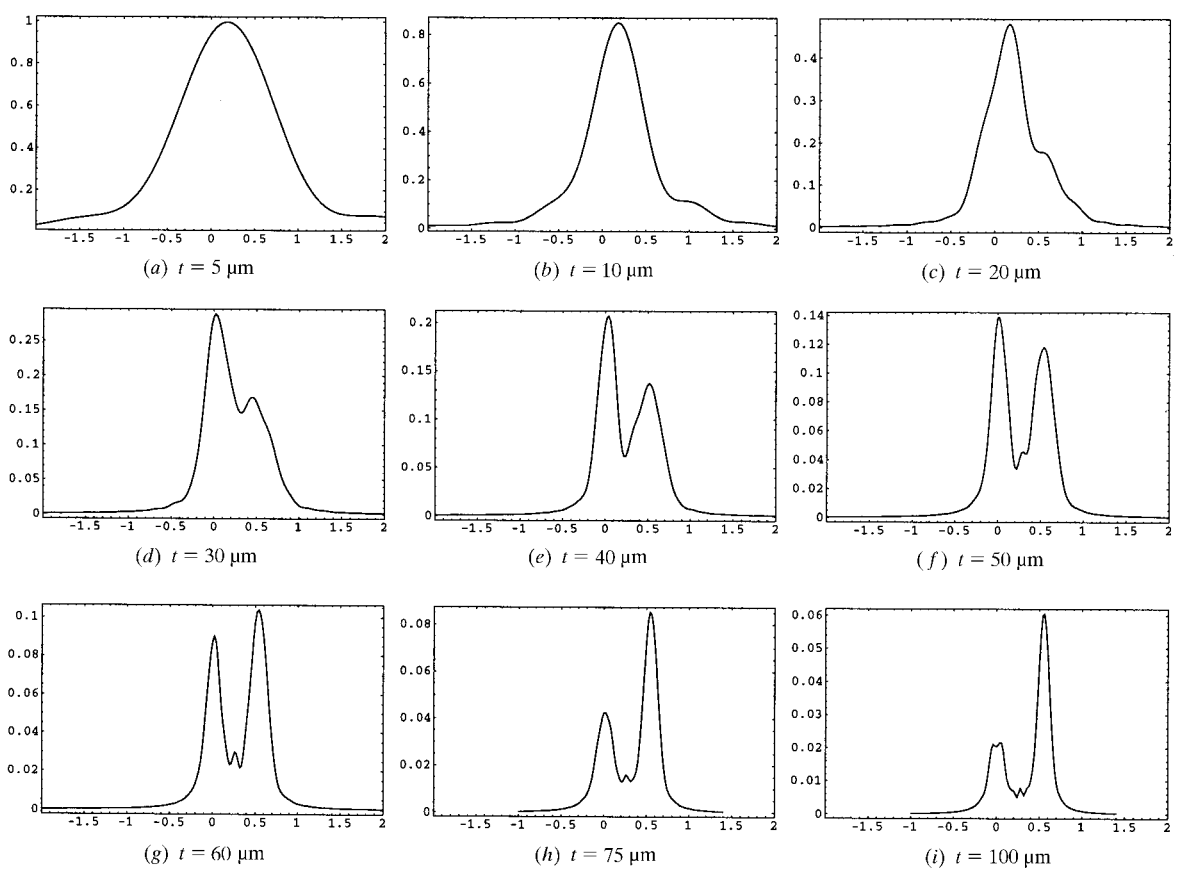

Fig. 15. Silicon (333), $t \times t$ crystal, varying t.

Related parameters:

$$\mu_L = \mu_\Lambda(\delta_+/\delta_-)^{1/2} \tag{50}$$

$$\Delta\mu_L = \mu_\Lambda \tfrac{1}{2}[(\delta_-/\delta_+)^{1/2} - (\delta_+/\delta_-)^{1/2}] \tag{51}$$

$$\mu_B = \mu_\Lambda \tfrac{1}{4}[(\beta_+/\beta_-)^{1/2} + (\beta_-/\beta_+)^{1/2}]. \tag{52}$$

APPENDIX *B*
Transition to standard results

We here briefly outline the equivalence between the results given in §2.2 and those obtained from the fundamental equation of dynamical theory. At this stage, $\Im\chi_o = 0$. Thus, Φ_0, μ_L, $\Delta\mu_L$ and μ_B are all zero.

*B*1. *Laue case*

The result from the Takagi theory is given in equation (16). We have to evaluate the integral ($\eta = \eta_L - \Delta\eta_L$):

$$I_L = \left| \xi_L \int_0^1 \mathrm{d}z\, J_0\{2\xi_L[(1-z)z]^{1/2}\} \exp(2i\xi_L\eta z) \right|^2.$$

With change of variable from z to $\bar{z}$,

$$z = \tfrac{1}{2}(1 + \bar{z}),$$

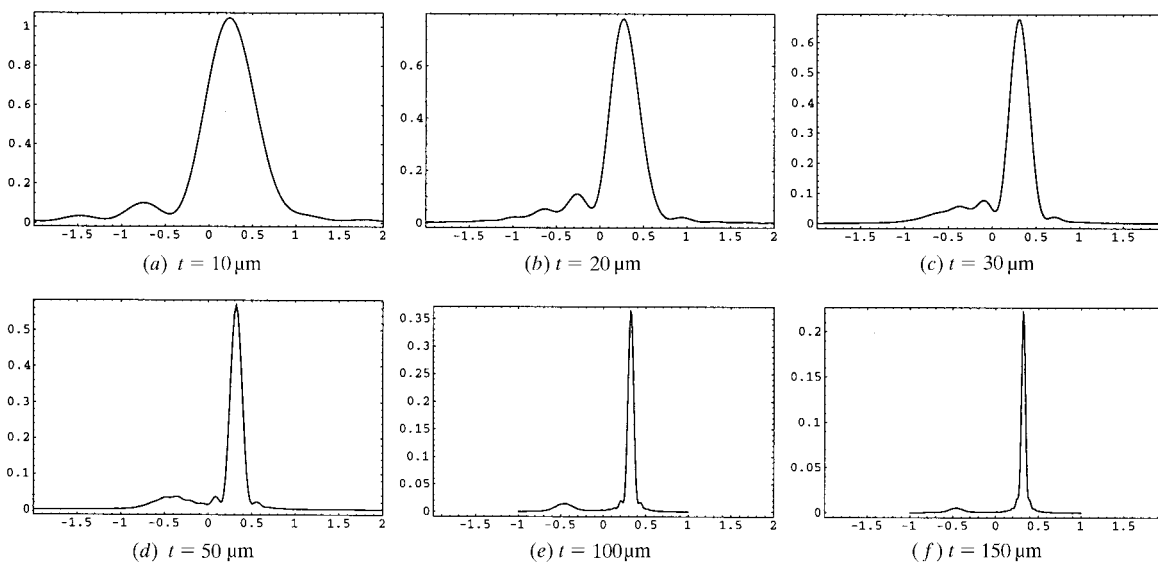

Fig. 16. Silicon (135), $\gamma = 28.561°$, $t \times t$ crystal, varying t.

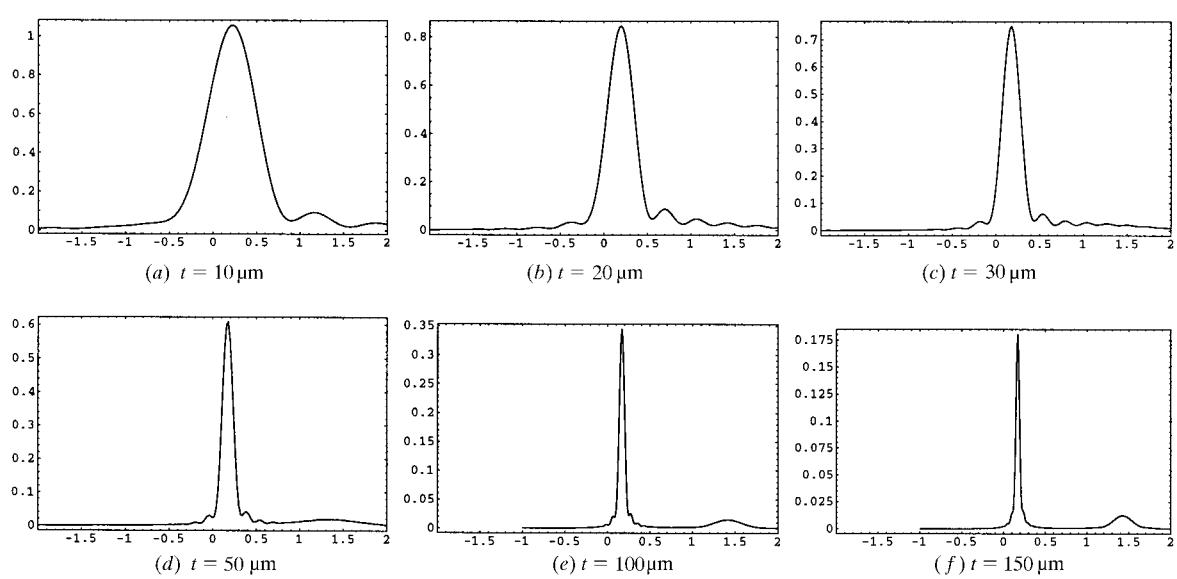

Fig. 17. Silicon (135), $\gamma = -28.561°$, $t \times t$ crystal, varying t.

we obtain

$$I_L = \left| \xi_L \int_0^1 \mathrm{d}\bar{z}\, J_0\left[\xi_L (1-\bar{z}^2)^{1/2}\right] \cos \xi_L \eta \bar{z} \right|^2 .$$

Using equation [6.677.6] of Gradshteyn & Ryzhik (1980) with $a = 1$, $b = \xi_L$ and $c = \xi_L \eta$, we have

$$I_L = \sin^2\, \xi_L (1+\eta^2)^{1/2}/(1+\eta^2).$$

Thus, in the case of a non-absorbing crystal, we find for the ratio of powers:

$$\frac{P_h}{P_o^{(e)}} = \frac{\delta_+}{\delta_-}\frac{I_h}{I_o^{(e)}} = \frac{\sin^2\, \xi_L (1+\eta^2)^{1/2}}{1+\eta^2}. \tag{53}$$

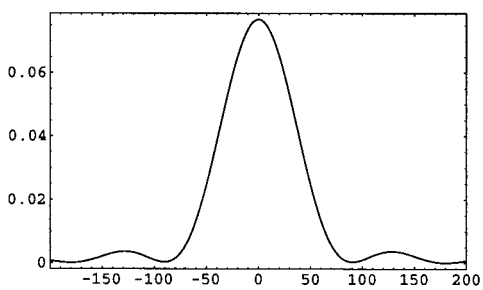

(*a*) 0.2 × 1.0 μm

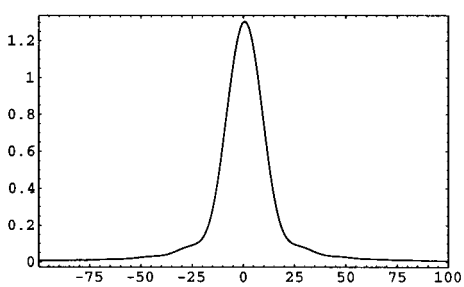

(*b*) 1.0 × 0.2 μm

Fig. 18. Silicon (111). Rocking curves in the kinematical limit.

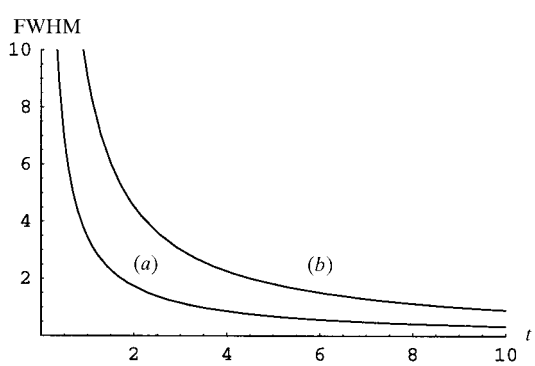

Fig. 19. Full width at half-maximum ($10^{-3\circ}$), for a $t \times t$ crystal as predicted by the kinematical theory, t in μm. (*a*) $\theta_{oh} = 30^\circ$, (*b*) $\theta_{oh} = 10^\circ$.

This is in agreement with Authier [1996, equations (5.1.6.6) and (5.1.6.7)].

B2. Bragg–Darwin case

Starting with equation (18), we have to evaluate the integral ($\eta = \eta_B - \Delta\eta_B$):

$$I_B = \left| \tfrac{1}{2} \int_0^\infty \mathrm{d}z\, [J_0(z) + J_2(z)] \exp(i\eta z) \right|^2 .$$

Using the identity

$$J_0(z) + J_2(z) = 2J_1(z)/z$$

and processing the tabulated integral equation [6.621.1] of Gradshteyn & Ryzhik (1980):†

$$\int_0^\infty [J_1(z)/z] \exp(i\eta z)\, \mathrm{d}z = \begin{cases} i\eta + (1-\eta^2)^{1/2} & |\eta| \le 1 \\ i\eta - i\,\mathrm{sign}[\eta](\eta^2-1)^{1/2} & |\eta| \ge 1, \end{cases} \tag{54}$$

we obtain for the ratio of powers:

$$\frac{P_h}{P_o^{(e)}} = \frac{\beta_+}{\beta_-}\frac{I_h}{I_o^{(e)}} = \begin{cases} 1 & |\eta| \le 1 \\ \left[|\eta| - (\eta^2-1)^{1/2}\right]^2 & |\eta| \ge 1, \end{cases} \tag{55}$$

which corresponds to the standard result of the fundamental theory for Bragg scattering from a 'thick' crystal [Authier, 1996, equation (5.1.7.1)].

B3. Bragg–Ewald case

Equation (21) is expressed by ($\eta = \eta_B - \Delta\eta_B$):

$$I_h = I_o^{(e)} (|\kappa_{ho}|/|\kappa_{oh}|)(\beta_-/\beta_+)|i_h(\xi_B)|^2$$

with

$$i_h(\xi_B) \stackrel{\mathrm{def}}{=} (\xi_B/2) \int_0^\infty \mathrm{d}z\, [J_0(\xi_B z) + J_2(\xi_B z)] \exp(i\eta\xi_B z) + (\xi_B/2) \sum_{p=1}^\infty \int_{2p}^\infty \mathrm{d}z\, w_h^{A-A}(\xi_B|z|2p) \exp(i\eta\xi_B z). \tag{56}$$

Using equation [6.646] of Gradshteyn & Ryzhik (1980):

$$\xi_B \int_{2p}^\infty \mathrm{d}z \left(\frac{z-2p}{z+2p}\right)^p J_{2p}\{\xi_B[z^2-(2p)^2]^{1/2}\} \exp(i\eta\xi_B z) = \begin{cases} \dfrac{\exp[-2p\xi_B(1-\eta^2)^{1/2}]}{(1-\eta^2)^{1/2}} \\ \quad \times [i\eta + (1-\eta^2)^{1/2}]^{2p} & |\eta| \le 1 \\ \dfrac{i\,\mathrm{sign}[\eta] \exp\{2p\xi_B\, \mathrm{sign}[\eta] i(\eta^2-1)^{1/2}\}}{(\eta^2-1)^{1/2}} \\ \quad \times \{i\eta - i\,\mathrm{sign}[\eta](\eta^2-1)^{1/2}\}^{2p} & |\eta| \ge 1. \end{cases}$$

† $\mathrm{sign}[\eta] = \eta/|\eta|$.

Here we analyse the case $|\eta| \leq 1$. A full account including $|\eta| > 1$ is given elsewhere (Thorkildsen & Larsen, 1998*d*). Introducing the functions $j(\xi_B; m)$:

$$\begin{aligned} j(\xi_B; m) &\stackrel{\text{def}}{=} \sum_{p=1}^{\infty} (-1)^p [i\eta + (1-\eta^2)^{1/2}]^{2(p+m)} \\ &\quad \times \exp[-2p\xi_B(1-\eta^2)^{1/2}] \\ &= [i\eta + (1-\eta^2)^{1/2}]^{2(m+1)} \{-1 + 2\eta^2 \\ &\quad - 2i\eta(1-\eta^2)^{1/2} - \exp[2\xi_B(1-\eta^2)^{1/2}]\}^{-1} \end{aligned}$$

and $J(\xi_B)$:

$$\begin{aligned} J(\xi_B) &\stackrel{\text{def}}{=} j(\xi_B; -1) + 2j(\xi_B; 0) + j(\xi_B; 1) \\ &= 4(-1+\eta^2)[1 - 2\eta^2 + 2i\eta(1-\eta^2)^{1/2}] \\ &\quad \times \{-1 + 2\eta^2 - 2i\eta(1-\eta^2)^{1/2} \\ &\quad - \exp[2\xi_B(1-\eta^2)^{1/2}]\}^{-1}, \end{aligned}$$

we find, using equation (54),

$$\begin{aligned} i_h(\xi_B) &= i\eta + (1-\eta^2)^{1/2} + J(\xi_B)/2(1-\eta^2)^{1/2} \\ &= \big[-i\eta + \big((1-\eta^2)^{1/2}\{1 + \exp[2\xi_B(1-\eta^2)^{1/2}]\}\big) \\ &\quad \times \{-1 + \exp[2\xi_B(1-\eta^2)^{1/2}]\}^{-1}\big]^{-1}. \end{aligned}$$

It follows that

$$\begin{aligned} |i_h(\xi_B)|^2 &= i_h^*(\xi_B) i_h(\xi_B) \\ &= \{-1 + \exp[2\xi_B(1-\eta^2)^{1/2}]\}^2 \\ &\quad \times \big(-4\eta^2 \exp[2\xi_B(1-\eta^2)^{1/2}] \\ &\quad + \{1 + \exp[2\xi_B(1-\eta^2)^{1/2}]\}^2\big)^{-1} \\ &= \sinh^2 \xi_B (1-\eta^2)^{1/2} \\ &\quad \times [1 - \eta^2 + \sinh^2 \xi_B (1-\eta^2)^{1/2}]^{-1}. \end{aligned}$$

In general,

$$\frac{P_h}{P_o^{(e)}} = \frac{\beta_+}{\beta_-}\frac{I_h}{I_o^{(e)}} = \begin{cases} \dfrac{\sinh^2 \xi_B (1-\eta^2)^{1/2}}{1 - \eta^2 + \sinh^2 \xi_B (1-\eta^2)^{1/2}} & |\eta| \leq 1 \\ \dfrac{\sin^2 \xi_B (\eta^2-1)^{1/2}}{\eta^2 - 1 + \sin^2 \xi_B (\eta^2-1)^{1/2}} & |\eta| \geq 1, \end{cases} \tag{57}$$

which is in accordance with the expressions given by Authier [1996, equations (5.1.7.6*a*) and (5.1.7.6*b*)].

Parts of this work have been presented at seminars in condensed matter physics at the ESRF, and at the annual meeting of the Norwegian Physical Society.

References

Afanasev, A. M. & Melkonyan, M. K. (1983). *Acta Cryst.* A**39**, 207–210.

Alexandrov, P. A., Afanasev, A. M. & Stepanov, S. A. (1984). *Phys. Status Solidi*, **86**, 143–154.

Authier, A. (1996). *International Tables for Crystallography*, Vol. B, edited by U. Shmueli, pp. 464–480. Dordrecht: Kluwer Academic Publishers.

Authier, A. & Simon, D. (1968). *Acta Cryst.* A**24**, 517–526.

Batterman, B. W. & Cole, H. (1964). *Rev. Mod. Phys.* **36**, 681–717.

Becker, P. (1977). *Acta Cryst.* A**33**, 667–671.

Becker, P. & Coppens, P. (1974). *Acta Cryst.* A**30**, 129–147.

Becker, P. & Dunstetter, F. (1984). *Acta Cryst.* A**40**, 241–251.

Coppens, P. (1992). *Synchrotron Radiation Crystallography*. New York: Academic Press.

Cromer, D. (1995). Private communication.

Cromer, D. & Liberman, D. (1970). *J. Chem. Phys.* **53**, 1891–1898.

Darwin, C. G. (1914). *Philos. Mag.* **27**, 675–690.

Ewald, P. P. (1916*a*). *Ann. Phys. (Leipzig)*, **49**, 1–38.

Ewald, P. P. (1916*b*). *Ann. Phys. (Leipzig)*, **49**, 117–143.

Ewald, P. P. (1917). *Ann. Phys. (Leipzig)*, **54**, 519–597.

Ewald, P. P. (1937). *Z. Kristallogr. Teil A*, **97**, 1–27.

Gradshteyn, I. S. & Ryzhik, I. M. (1980). *Table of Integrals, Series, and Products*. New York: Academic Press.

Holý, V. (1996). *Proceedings, X-ray and Neutron Dynamical Diffraction. Theory and Applications*, edited by A. Authier, S. Lagomarsino & B. Tanner, *NATO ASI Series Series B: Physics*, Vol. 357, pp. 33–42. New York: Plenum.

James, R. W. (1962). *The Optical Principles of the Diffraction of X-rays*. London: Bell.

Kato, N. (1974). *X-ray Diffraction*, ch. 4. New York: McGraw-Hill.

Kato, N. (1992). *Acta Cryst.* A**48**, 829–834.

Larsen, H. B. & Thorkildsen, G. (1998). *Acta Cryst.* A**54**, 511–512.

Laue, M. von (1931). *Ergebn. Exact. Naturwiss.* **10**, 133–158.

Laue, M. von (1960). *Röntgenstrahlinterferenzen*. Frankfurt am Main: Akademische Verlagsgesellshaft.

Olekhnovich, N. M. & Olekhnovich, A. I. (1978). *Acta Cryst.* A**34**, 321–326.

Olekhnovich, N. M. & Olekhnovich, A. I. (1980). *Acta Cryst.* A**36**, 22–27.

Pinsker, Z. G. (1978). *Dynamical Scattering of X-rays in Crystals*. Berlin: Springer-Verlag.

Prins, J. A. (1930). *Z. Phys.* **63**, 477–493.

Saka, T., Katagawa, T. & Kato, N. (1972*a*). *Acta Cryst.* A**28**, 102–113.

Saka, T., Katagawa, T. & Kato, N. (1972*b*). *Acta Cryst.* A**28**, 113–120.

Saka, T., Katagawa, T. & Kato, N. (1973). *Acta Cryst.* A**29**, 192–200.

Sommerfeld, A. (1949). *Partial Differential Equations*. New York: Academic Press.

Takagi, S. (1962). *Acta Cryst.* **15**, 1311–1312.

Takagi, S. (1969). *J. Phys. Soc. Jpn*, **26**, 1239–1253.

Taupin, D. (1964). *Bull. Soc. Fr. Minéral. Cristallogr.* **87**, 469–511.

Thorkildsen, G. & Larsen, H. B. (1998*a*). *Acta Cryst.* A**54**, 172–185.

Thorkildsen, G. & Larsen, H. B. (1998*b*). *Acta Cryst.* A**54**, 186–190.

Thorkildsen, G. & Larsen, H. B. (1998*c*). *Acta Cryst.* A**54**, 416–429.

Thorkildsen, G. & Larsen, H. B. (1998*d*). *Two Beam Diffraction in Perfect Crystals Analyzed by Takagi's Equations.* Part 3. *Rocking Curves & Intensity Distributions.* Technical Report 42. Stavanger College, Stavanger, Norway.
Thorkildsen, G. & Larsen, H. B. (1999). *Acta Cryst.* A**55**, 1–13.
Uragami, T. S. (1969). *J. Phys. Soc. Jpn*, **27**, 147–154.
Uragami, T. S. (1970). *J. Phys. Soc. Jpn*, **28**, 1508–1527.
Uragami, T. S. (1971). *J. Phys. Soc. Jpn*, **31**, 1141–1161.
Waasmaier, D. & Kirfel, A. (1995). *Acta Cryst.* A**51**, 416–431.
Wilkins, S. W. (1978). *Proc. R. Soc. London Ser A*, **364**, 569–589.
Wilkins, S. W. (1981). *Philos. Trans. R. Soc. London*, **299**, 275–317.
Wolfram, S. (1996). *The Mathematica Book*, 3rd ed. Champain, IL 61820, USA: Wolfram Media/Cambridge University Press.
Zachariasen, W. H. (1945). *Theory of X-ray Diffraction in Crystals.* London: Wiley.
Zachariasen, W. H. (1967). *Acta Cryst.* **23**, 558–564.